Infrared Physics & Technology 54 (2011) 170–176

Contents lists available at ScienceDirect

Infrared Physics & Technology

journal homepage: www.elsevier.com/locate/infrared

C-QWIPs for space exploration

K.K. Choi [a,*], M.D. Jhabvala [b], D.P. Forrai [c], J. Sun [a], D. Endres [c]

[a] US Army Research Laboratory, Adelphi, MD 20783, USA
[b] NASA Goddard Space Flight Center, Greenbelt, MD 20771, USA
[c] L3-Cincinnati Electronics, Mason, OH 45040, USA

ARTICLE INFO

Article history:
Available online 25 December 2010

Keywords:
QWIP
FPA
NEΔT

ABSTRACT

We have extended our investigation of corrugated quantum well infrared photodetector focal plane arrays (C-QWIP FPAs) into the far infrared regime. Specifically, we are developing the detectors for the thermal infrared sensor (TIRS) used in the NASA Landsat Data Continuity Mission. This mission requires infrared detection cutoff at 12.5 μm and FPAs operated at ~43 K. To maintain a low dark current in these extended wavelengths, we adopted a low doping density of 0.6×10^{18} cm^{-3} and a bound-to-bound state detector in one of the designs. The internal absorption quantum efficiency η is calculated to be 25.4% for a pixel pitch of 25 μm and 60 periods of QWs. With a pixel fill factor of 80% and a substrate transmission of 70.9%, the external η is 14.4%. To yield the theoretical conversion efficiency CE, the photoconductive gain was measured and is 0.25 at 5 V, from which CE is predicted to be 3.6%. This value is in agreement with the 3.5% from the FPA measurement. Meanwhile, the dark current is measured to be 2.1×10^{-6} A/cm^2 at 43 K. For regular infrared imaging above 8 μm, the FPA will have a noise equivalent temperature difference (NETD) of 16 mK at 2 ms integration time in the presence of 260 read noise electrons, and it increases to 22 mK at 51 K. The highest operability of the tested FPAs is 99.967%. With the CE agreement, we project the FPA performance in the far infrared regime up to 30-μm cutoff, which will be useful for the Jupiter-Europa deep space exploration. In this work, we also investigated the C-QWIP optical coupling when the detector substrate is thinned.

Published by Elsevier B.V.

1. Introduction

We have developed the corrugated quantum well infrared photodetector focal plane array (C-QWIP FPA) technology for a number of years. At present, both the theoretical model and the production processes are sufficiently mature such the FPA properties are well understood in the quantitative manner while high production yield is consistently maintained. In this work, we applied this technology to the NASA Landsat project and obtained satisfactory results. In view of the agreement between theory and experiment in these and other detectors in the long wavelength regime, we extend the C-QWIP model to the far infrared and predict its performance up to 30-μm cutoff. In this work, we also perform a three-dimensional (3D) finite element electromagnetic (EM) field simulation to investigate the effects of substrate thickness on the C-QWIP optical properties.

2. TIRS5 FPA

In this section, we apply the classical geometric-optical (GO) C-QWIP model [1] to one of the FPAs developed for a thermal infrared sensor (TIRS) instrument [2]. To predict the external quantum efficiency η of a C-QWIP FPA, the absorption coefficient $\alpha(\lambda)$ of the QWIP material is first calculated for parallel propagating light with a proper polarization. $\alpha(\lambda)$ is given by

$$\alpha(\lambda) = \sum_n \frac{N_D W}{L} \frac{\pi e^2 \hbar}{2\sqrt{\varepsilon_h}\varepsilon_0 m^* c} f_n \rho_n(\lambda), \tag{1}$$

where N_D is the doping density in the well, W is well width, L is the QW period length, f_n is the oscillator strength from the ground state to the nth excited state, and ρ_n is the normalized Gaussian broadening for each optical transition. The values of f_n are obtained after solving the eigen energies and eigen functions of the structure. The C-QWIP pixel structure reflects the normally incident light into parallel propagation, with which η under the GO model is given by

$$\eta(V,\lambda) = t_s f_p \eta_{\text{int}} = t_s f_p \kappa \frac{1}{p}\left[t + \frac{e^{-\alpha p}}{2\alpha}(1 - e^{2\alpha t})\right]\gamma(V). \tag{2}$$

In Eq. (2), t_s is the substrate transmission, f_p is the pixel fill factor, η_{int} is the internal quantum efficiency, κ is a factor proportional to the thickness of the active layer inside a corrugation [1], p is the pixel linear dimension, t is the corrugation height, and

* Corresponding author. Tel.: +1 301 394 0495; fax: +1 301 394 1157.
E-mail address: kwongkit.choi@us.army.mil (K.K. Choi).

1350-4495/$ - see front matter Published by Elsevier B.V.
doi:10.1016/j.infrared.2010.12.006

$\gamma(V)$ is the transmission coefficient of a photoelectron traveling out of the QW at a bias V. The resulting photocurrent J_p generated within a C-QWIP pixel is then

$$J_p(V,T_B)=\frac{\pi}{4F^2+1}eg(V)\int_{\lambda_1}^{\lambda_2}\eta(V,\lambda)L(T_B,\lambda)d\lambda, \tag{3}$$

where T_B is the scene temperature, $g(V)$ is the photoconductive gain obtained from noise measurement, λ_1 and λ_2 are the lower and upper wavelengths encompassing the detector absorption spectrum, F is the f-number of the optical system, and $L(T_B, \lambda)$ is the photon spectral radiance.

The QWIP material described in this section is labeled as TIRS5. It is made of 60 periods of 700-Å $Al_{0.172}Ga_{0.828}As$ and 60-Å GaAs. To avoid dopant migration during the material growth, only the center part of the well is doped such that the equivalent N_D is 0.6×10^{18} cm^{-3} in the well. The active QW material is sandwiched between two GaAs contact layers. The top layer is 3.67 μm thick and the bottom layer is 4.15 μm thick. Applying Eq. (1) to this material, the value of α is shown in Fig. 1. Its peak value is 0.17 μm^{-1}. The calculation shows that the structure is a bound-to-bound (B–B) state detector because its peak is below the barrier height. The combination of a low doping density and the B–B detector structure ensures a low dark current for this long wavelength detector.

Inserting $\alpha(\lambda)$ into Eq. (2), η_{int} and η can be obtained. With $p=25$ μm, $t=11$ μm and $K=0.69$ for 60 QWs, the peak η_{int} is 25.4%. For the present uncoated FPA, $t_s=0.709$, and assuming $f_p=0.80$ and $\gamma=1$ at high bias, the calculated external η is shown in Fig. 2 with a peak value of 14.4%. To know the external conversion efficiency CE ($\equiv\eta g$), the photoconductive gain $g(V)$ was obtained from the noise measurement and is shown in Fig. 3. At the substrate bias of 5 V, g was measured to be 0.25, with which the peak CE is predicted to be 3.6%. The material was processed into C-QWIP FPAs and the arrays were hybridized to Indigo 9803 640×512 readout circuits (ROICs). The measured CE from one of the FPAs is shown in Fig. 4. It increases with the applied bias, and at 5 V, it was measured to be 3.5%, agreeing with the prediction at 3.6%. The dashed curve in Fig. 4 is the same curve shown in Fig. 2 but was shifted to a shorter wavelength by 0.35 μm to match the experimental spectrum. From the agreements on both the magnitude and lineshape, one can assess the accuracy of the detector model in predicting the C-QWIP optical properties. Using the fitted CE spectrum (dashed curve in Fig. 4), the calculated detector photocurrent from Eq. (3) is 1.19×10^{-4} A/cm^2 (or 4.62×10^9 e/s/pixel) with $F/2$ optics and 294 K background when imaging at $\lambda>8$ μm.

In addition to the optical properties, the dark current of a C-QWIP can also be modeled and predicted in sufficient accuracy.

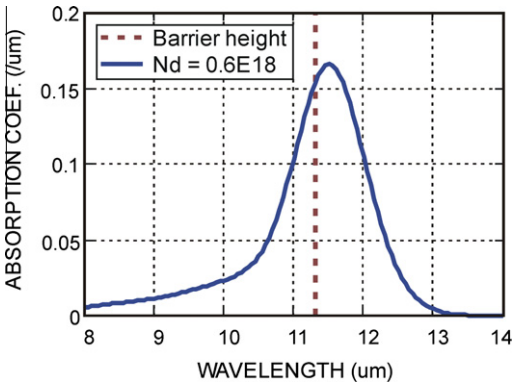

Fig. 1. The calculated absorption coefficient α of TIRS5. The straight line divides B–B transitions on the right and bound-to-continuum transitions on the left.

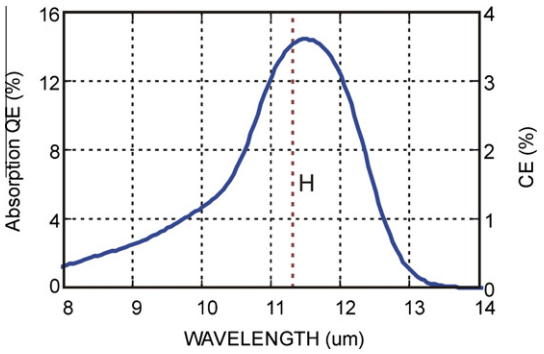

Fig. 2. The calculated η and CE spectra of TIRS5 for $g=0.25$.

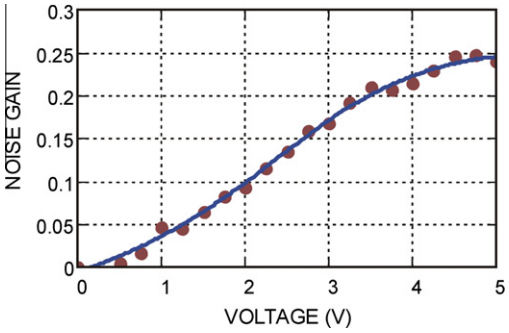

Fig. 3. The photoconductive gain of TIRS5 obtained from noise measurement.

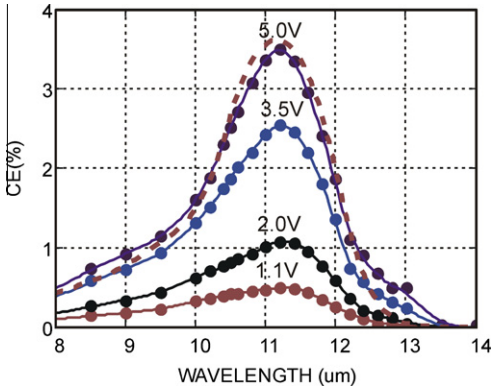

Fig. 4. The measured spectral conversion efficiency of a TIRS5 FPA at different bias (circles) and the calculated CE (dashed curve) at 5 V, which has been blue shifted by 0.35 μm.

The dark current transport can be classified into three main mechanisms, which are direct tunneling (DT) between adjacent QWs, thermally assisted tunneling (TAT) near the tip of a tilted barrier under bias, and thermionic emission (TE) over the barrier. All of these three transport mechanisms can be incorporated into a single expression [3], in which

$$\begin{aligned}J(V,T)&=\int_{E_1}^{\infty}J(E,V,T)dE,\\&=\int_{E_1}^{\infty}e\rho f(E,T)\gamma(E,V)v(V)dE,\\&=\int_{E_1}^{\infty}e\frac{m^*}{\pi\hbar^2L}\frac{\gamma(E,V)}{1+\exp\left(\frac{E-E_F-E_1}{kT}\right)}\frac{\mu V/L}{\sqrt{1+\left(\frac{\mu V}{Lv_{\text{sat}}}\right)^2}}dE.\end{aligned} \tag{4}$$